

In-Situ X-Ray Characterization of Fiber Structure During Melt Spinning

Michael S. Ellison, Ph.D.¹, Paulo E. Lopes, Ph.D.², William T. Pennington, Ph.D.³

¹School of Materials Science & Engineering, and Center for Advanced Engineering Fibers and Films (CAEFF), Clemson University, Clemson, South Carolina, USA

²Center for Advanced Engineering Fibers and Films (CAEFF), and Department of Chemistry, Clemson University, Clemson, South Carolina, USA

³Department of Chemistry, and Center for Advanced Engineering Fibers and Films (CAEFF), Clemson University, Clemson, South Carolina, USA

Correspondence to:

Michael S. Ellison email: ellisom@clemson.edu

ABSTRACT

The properties of a polymer are strongly influenced by its morphology. In the case of fibers from semi-crystalline polymers this consists of the degree of crystallinity, the spacing and alignment of the crystalline regions, and molecular orientation of the polymer chains in the amorphous regions. Information on crystallinity and orientation can be obtained from X-ray analysis. In-situ X-ray characterization of a polymer during the melt spinning process is a major source of information about the effects of material characteristics and processing conditions upon structure evolution along the spinline, and the final structure and properties of the end product.

We have recently designed and installed an X-ray system capable of in-situ analysis during polymer melt spinning. To the best of our knowledge this system is unique in its capabilities for the simultaneous detection of wide angle and small angle X-ray scattering (WAXS and SAXS, respectively), its use of a conventional laboratory radiation source, its vertical mobility along the spinline, and its ability to simulate a semi-industrial environment.

Setup, operation and demonstration of the capabilities of this system is presented herein as applied to the characterization of the melt spinning of isotactic poly(propylene). Crystallinity and crystalline orientation calculated from WAXS patterns, and lamellar long period calculated from SAXS patterns, were obtained during melt spinning of the polymer along the spinline.

INTRODUCTION

Polymers, particularly semi-crystalline polymers, can possess a wide range of properties depending on the processing conditions. Polymer fibers are commonly formed by melt spinning of semi-crystalline polymers, where their structure develops during the processes of spinning and of post drawing. Subsequent to exiting the spinneret, the fiber is cooled by heat transfer from the surface of the fiber to the surrounding air. Along the spinline, the polymer filament velocity increases from that at the face of the spinneret (the throughput rate) to that of the speed of the take-up winder. The fiber decreases in diameter until the point in the spinline where both the diameter and the velocity become constant. Orientation of the polymer chains increases due to elongational (spinline) stress on the filament. The primary contributor to this stress is the rheological force, which has its basis in the viscosity of the polymer. The decrease in entropy associated with uncoiling of the chains as they assume the oriented conformation contributes to this force. Inasmuch as viscous forces are inherently deformation rate-dependent, the spinline stress increases with increase in spinning velocity; hence, we observed an increase in orientation with increase in spinning speed. Crystallization occurs in appropriate polymers during cooling; in the case of sufficiently high take-up speeds, crystallinity may be influenced by the speed-induced stress.¹

In the case of fibers from crystallizable polymers, the parameters describing the internal structure of the fiber include the degree of crystallinity and crystallite orientation, the spacing and arrangement of the crystalline regions, and molecular orientation of the

polymer chains in the amorphous regions. X-ray studies of polymers provide different information depending on the nature of the polymer, viz. whether amorphous or semi-crystalline, and on the technique used, wide-angle X-ray scattering (WAXS) or small angle X-ray scattering (SAXS).²⁻⁵

In order to develop models to describe, at the molecular and continuum levels, the effect of material properties and processing conditions upon the structure and properties of an end product, measurements to verify model predictions against experimental data are critical. X-ray techniques have long been applied to the study of polymer structure and ex situ techniques are commonly used to relate structure with processing conditions.⁶⁻¹⁵ A more challenging approach is to conduct in situ X-ray measurements along the spinline. The first in situ X-ray application for the characterization of a polymer spinline was the work of Katayama, *et al.*,¹⁶ studying the melt spinning of low density poly(ethylene), high density poly(ethylene), poly(propylene) and poly(butene-1). In the 1970s Spruiell, White and co-workers published a series of works reporting on the study of structure development during the melt spinning of poly(ethylene),^{7,9} poly(propylene),^{10,11} and poly(amide 6).¹² Later Haberkorn, *et al.*¹⁷ studied poly(amide 6) and poly(amide 6,6) melt spinning at high take-up speeds, and Hsiao, *et al.*¹⁸ presented work on the characterization of melt spinning and post-drawing processes of poly(amide 6,6).

The use of higher flux synchrotron X-ray sources to study structure development in the spinline of polymer melt spinning was first reported in 1993 by Cakmak *et al.*¹⁹ on poly(vinylidene fluoride) tapes. In 1998 Terril *et al.*²⁰ presented a study on poly(propylene), and studies on poly(amide 6),²¹ poly(vinylidene fluoride) fibers,²² poly(butene-1),²³ poly(propylene),²⁴ poly(ethylene terephthalate),²⁵ poly(ethylene),²³⁻²⁶ and poly(oximethylene)²⁷ have since been reported by several authors in the following years. The works of Cakmak and of Terrill were conducted at the Synchrotron Radiation Source (SRS) at the CCLRC Daresbury Laboratory in Warrington, United Kingdom, and all others were conducted at the Hamburg Synchrotron Radiation Laboratory (HASYLAB) at the Deutsches Elektronen-Synchrotron (DESY) in Hamburg, Germany.

The initial applications of in-situ X-ray for polymer process characterization were conducted using rotating anode X-ray generators^{7, 9, 12, 16} to obtain the

highest possible beam intensity from a laboratory source in order to reduce the time required to obtain a pattern, in this respect the synchrotron X-ray sources have the advantage, taking from a few seconds to one minute to obtain a pattern,¹⁸⁻²⁵ compared to several hours in the former systems. Both X-ray sources, rotating anode and synchrotron, presented the inconvenience of a fixed beam line, so the extruder had to be moved to allow the X-ray beam to reach different positions on the spinline. This motion was achieved by moving only the top part of the extruder with the consequence of changing the length of the spinline. Only the work of Haberkorn, *et al.*¹⁷ and Hsiao, *et al.*¹⁸ were conducted without changing the geometry of the spinline during the course of the measurements.

In-situ X-ray techniques therefore provide an invaluable tool for the characterization of structure development during polymer processing; thus, instrumentation capable of the simultaneous detection of wide angle and small angle X-ray scattering has recently been designed and installed in our facilities to support the efforts of the Center for Advanced Engineering Fibers and Films (CAEFF) at Clemson University²⁸. To the best of our knowledge, this system is unique in its use of a conventional laboratory radiation source and its vertical mobility along the spinline to provide capabilities for simultaneous detection of WAXS and SAXS during pilot scale fiber production. In conjunction with the XRD system, additional capability for in-situ measurement of fiber diameter, velocity, and temperature, provide a very detailed description of spinline parameters during melt-spinning. The crystalline forms present in polypropylene, which is the subject of this investigation, are known. The information reported here, through in situ X-ray analysis, includes the identification of the crystalline forms present, quantification of the amount of crystalline material, the size of the crystallites, evaluation of preferred orientation, and dimension of lamellar structure. Our objective is to demonstrate the efficacy of this semi-industrial scale on-line XRD system.

EXPERIMENTAL

Materials

The polymer studied was isotactic poly(propylene) (iPP) reference Pro-fax PCD 1267 supplied by Basell. PCD 1267 is a high melt flow index poly(propylene) homopolymer designed for fiber spinning. The melt flow index for this polymer is 18

g/10 min (230°C /2.16 kg - ASTM Method D 1238), according to the manufacturer.

Extruder

A pilot scale polymer extruder, manufactured by Alex James, Inc., of Greenville, SC was used for melt-spinning of iPP. The extruder had a 15" long 5/8" diameter screw corresponding to a L/D ratio of 24/1. The screw enclosure, or barrel, and the spinning head were provided with independent heating elements set incrementally from 150° to the final spinning temperature of 220° C. The extruder screw rotation, which forces the polymer melt through the extruder, was controlled by the pressure set point at 200 psi. The flow of the polymer melt through the spinneret was controlled by a metering pump installed in the extruder head with a capacity of 0.297 cm³rev⁻¹. Throughput rates of 0.3, 0.6, and 1.2 cm³min⁻¹hole⁻¹ were used.

The spinneret had 6 holes of 1 mm diameter with L/D = 3 and entrance angle of 30°. Room temperature air was blown at 1 m s⁻¹ from a quench tower to cool the filaments. The take-up speeds of 50, 100, 200, and 400 m min⁻¹ were controlled by the take-up roll, located 202 cm below the spinneret.

X-Ray System for In-Situ Characterization of Polymer Fibers

The X-ray system was installed along the spinline of a pilot scale extruder. In order to be able to explore the spinning line at different distances from the exit of the spinneret, the X-ray source and detectors are mounted on a platform that can be moved vertically over distances ranging from 8.0 to 68.5 cm from the exit of the spinneret (*Figures 1 and 2*) in 1.0 mm steps.

A monochromatic X-ray beam (CuK α_1 , $\lambda = 1.5406$ Å) with a diameter of 0.5mm at the sample (approximately 70 cm from the X-ray source) was provided by a Micromax 2® X-ray generator (Osmic, Inc.), equipped with a Microsource® X-ray tube (Bede Scientific Instruments Ltd), coupled with a two-dimensional multilayer optics system (Microfocus Confocal Max-Flux Optic (μCMF)®). The X-ray beam exited the tube and passed through an external shutter then passed through a 173 mm pinhole collimator, with a front aperture of either 0.3 or 0.5 mm. The collimator can be fitted with a rear aperture of 0.3, 0.5, or 1 mm, or used without a rear aperture. The beam path from the source to the front of the collimator was flushed with helium, to improve the beam intensity. The sample was placed at a

distance of approximately 1.5 cm from the collimator, and two video cameras, focused at the intersection of the X-ray beam and the sample in the spinline, allowed correct positioning of the sample in the beam.

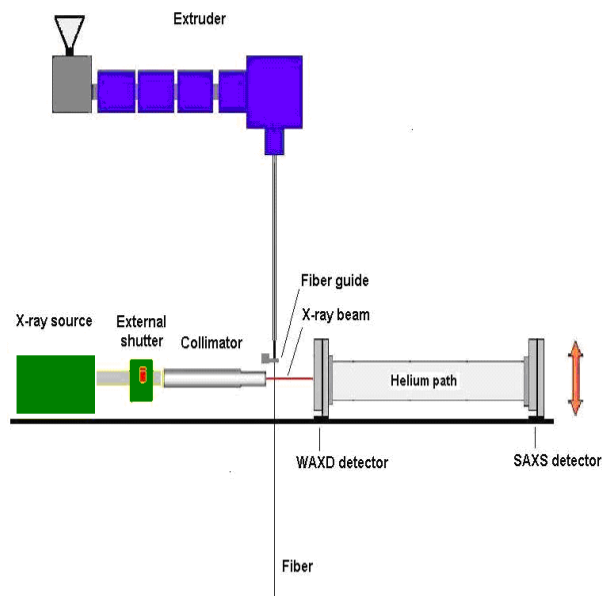


Figure 1. Schematic of the X-ray system, extruder, and in-situ fiber

Image plates (IP's; Fujifilm BAS-IP MS2325) were used for detection of the X-ray scattering, one at 10 cm from the sample to monitor WAXS, and another at 100.0 cm to monitor SAXS (*Figure 1*). For the simultaneous detection of WAXS and SAXS a 1.2 cm hole cut in the WAXS plate allowed the SAXS signal to pass through to an 85.0 cm helium-filled beam chamber which ended at the SAXS IP. A beam stop, 1 cm in diameter, was mounted just in front of the small-angle IP holder.

Handling of the IP's between the stages of exposure scanning and erasure is performed by a Mitsubishi RV-E2 robot mounted on a sled with a CR-E116 robot controller. The IP's are secured to the robot hand and to the IP holders by vacuum. The motion of the robot sled, and of the vertical platform, is performed by two Sanyo Denki servo motors and controllers. Movement of the IP holders between the expose and transfer positions, the opening and closing of the IP trays, the eraser tray, and the scanner lid, is done by compressed air or nitrogen, and regulated by pneumatic actuators.

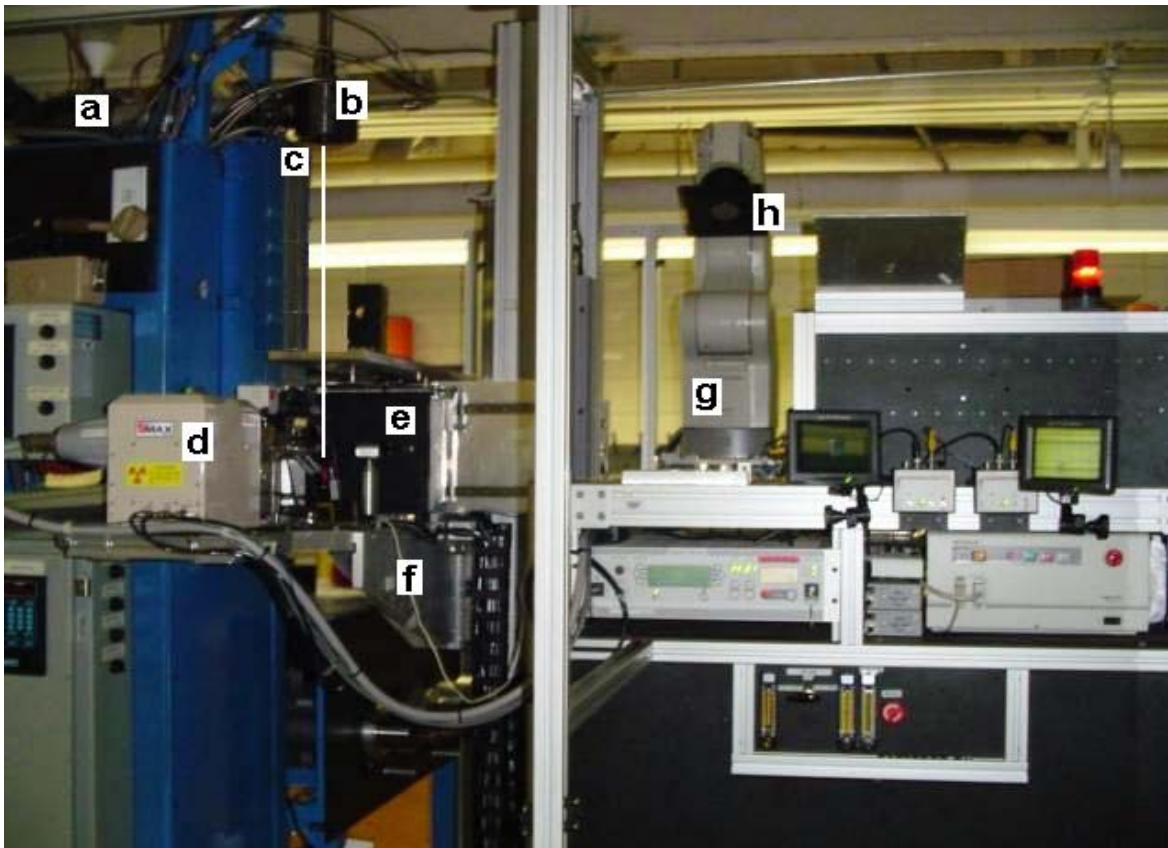


Figure 2. Photograph of the X-ray system: (a) extruder; (b) spinhead containing gear pump and spinneret; (c) line depicting filament path; (d) X-Ray tube; (e) wide-angle IP; (f) elevator platform; (g) robot; (h) robot arm with IP holder.

All operations of the X-ray system involving the platform, the robot, the external shutter, safety interlocks on the X-ray cabinet doors, and the scanner were controlled and integrated by the X-ray control software, *Spectre*.²⁹ *Spectre* also controls the startup and initialization of the I/O board, and handles communications between the I/O board and the robot controller, the motion controllers, and the scanner. In addition, *Spectre* schedules experimental runs and controls the sequence of operations during a run.

Multiple filaments were used for the X-ray determinations, to increase the volume of sample in the X-ray beam path. Spatial stability of the filaments during X-ray data collection was achieved through use of a Teflon coated ‘pig tail’ guide (*Figure 3*) which was placed either above or below the intersection of the X-ray beam and the spinline. Preferentially the guide was placed above the intersection to provide better alignment of the filaments in the beam, but at positions close to the

spinneret exit this was not always possible due to the high temperature of the polymer melt (fiber not yet solid), which makes the fibers too sticky to allow use of the guide. The additional surface friction drag associated with the guide is presumed minimal; also, it was always present, so any effect on spinline dynamics is relatively consistent across runs. The alteration of the spinline stress associated with the guide may induce a slight shift in position of parameter values along the spinline. This shift is presumed negligible.

For the experiments described here, the X-ray generator was set to operate at 45kVA and 0.67mA (3.35 W). The 0.5 mm collimator with 0.5 mm rear aperture was the configuration used throughout this work. WAXS and SAXS diffraction patterns were obtained at distances of 15, 30, 45, and 60 cm from the spinneret exit.

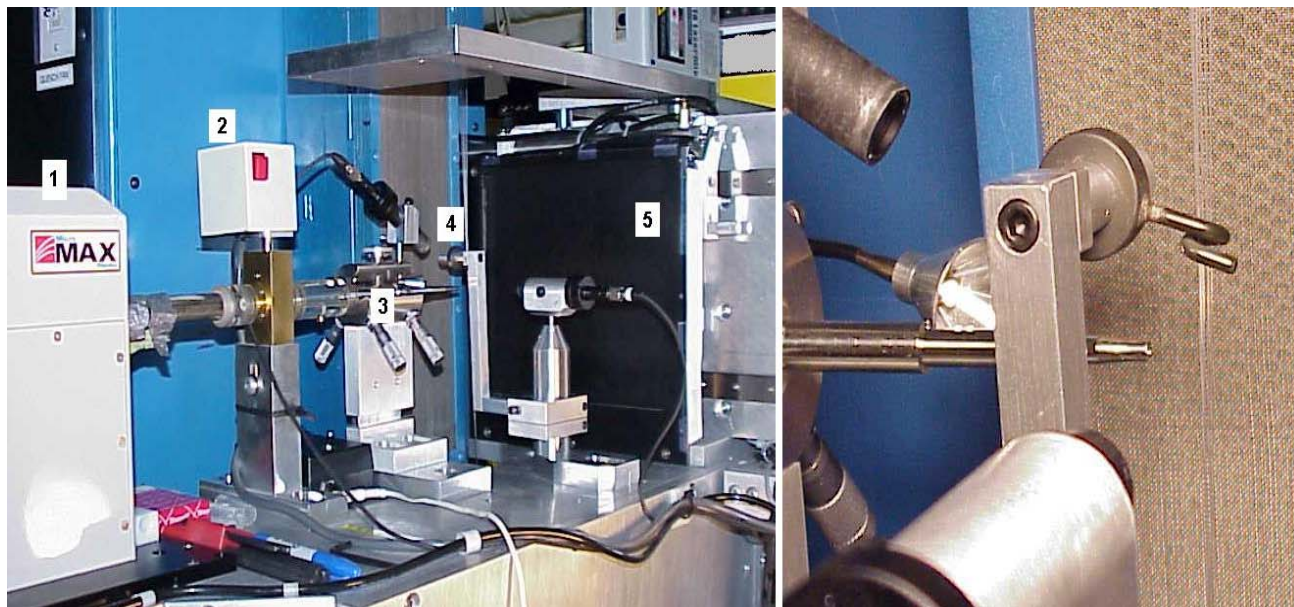


Figure 3. Sample positioning in the X-ray beam. General view (left) showing: (1) X-ray source; (2) external shutter; (3) collimator; (4) fiber guide; (5) WA detector. Close-up view (right) of the filaments passing through the fiber guide.

The exposure time to obtain a WAXS and SAXS pattern was typically 20 min. The IP's were scanned with a resolution of 200 μm per pixel. Background patterns corresponding to the scattering of the X-ray beam by air were obtained at equal lengths of time and used in the data processing. Position of the platform, exposure time, loading and scanning of the IP's, were controlled by the *Spectre* application, and based on the experimental sequence.

Data Processing

The *Polar* software application³⁰ was used for processing and analysis of the two dimensional X-ray intensity distributions to obtain structural information such as crystallinity and orientation parameters from WAXS, and lamellar thickness from SAXS.

After finding the center of the pattern and subtraction of the background scattering the crystallinity index, C , is calculated as:

$$C = (V_{\text{Tot}} - V_{\text{Amor}}) / V_{\text{Tot}} = (V_{\text{Tot}} - 2\pi p \int_{s_0}^{s_1} s^2 I_A^0(s) \sin \phi ds) / V_{\text{Tot}} \quad (1)$$

where $I_A^0(s)$ is the isotropic intensity (minimum intensity from the fitting), p is the "contribution from amorphous to the minimum" parameter, and:

$$V_{\text{Tot}} = 2\pi \int_{s_0}^{s_1} \int_0^\pi s^2 I(s, \phi) \sin \phi d\phi ds \quad (2)$$

Orientation is calculated as:

$$\langle \cos^2 \phi \rangle = \left(\int_0^{\pi/2} I(s, \phi) \cos^2 \phi \sin \phi d\phi \right) / \left(\int_0^{\pi/2} I(s, \phi) \sin \phi d\phi \right) \quad (3)$$

$f_2(s)$, the Herman's orientation factor is related to $\langle \cos^2 \phi \rangle$ as:

$$f_2(s) = (3 \langle \cos^2 \phi \rangle - 1) / 2 \quad (4)$$

The calculation of the c axis orientation (chain direction) of the monoclinic α form was calculated from the orientation of the 110 and 040 peaks,^{4, 31, 32} using the relation:

$$f_{c,z} = (3 \langle \cos^2 \phi_{c,z} \rangle - 1) / 2 \quad (5)$$

where:

$$\langle \cos^2 \phi_{c,z} \rangle = 1 - 1.099 \langle \cos^2 \phi_{110,z} \rangle - 0.901 \langle \cos^2 \phi_{040,z} \rangle \quad (6)$$

The SAXS patterns present some noise in the top half of the image plate which arise from edge scattering from the beam stop, due to use of the 0.5 mm collimator. Consequently, all calculations from small angle data are performed using the bottom half of the pattern. Due to the presence of lamellar structures the

small angle patterns are anisotropic, and marked by the presence of the two point pattern in the meridian. From the plot of the Lorentz corrected intensity profiles $I(s)*s^2$ vs. s , the value s_{max} was obtained corresponding to the maximum of the intensity distribution. The long period (L_p) of the lamellar structure was calculated from the position of the maximum using the Bragg relation as:

$$L_p = 1/s_{max} \quad (7)$$

RESULTS AND DISCUSSION

WAXS Patterns

Wide angle X-ray patterns were analyzed to reveal the presence of crystalline material, the degree of crystallinity, and the existence of preferred orientation of the crystalline material as a function of variables such as: distance from the exit of the spinneret, take-up speed, and throughput rates. The quantitative evaluation of crystallinity and c-axis orientation for the patterns discussed are presented in *Table I*.

Distance from the exit of the spinneret

Wide angle X-ray patterns obtained at different distances from the exit of the spinneret, for all experimental conditions, show evident qualitative changes in the crystallinity and crystalline orientation of the polymer. A set of WAXS patterns obtained at different distances from the spinneret at the

throughput rate of $0.6 \text{ cm}^3\text{min}^{-1}\text{hole}^{-1}$ and take-up speed of 100 m min^{-1} are presented in *Figure 4*, and the corresponding integrated intensity profiles are plotted in *Figure 5*. These patterns and plots show the presence of a typical amorphous pattern at a distance of 15 cm, and from 30 cm onwards the patterns reveal the presence of crystalline material, with crystallinity increasing with distance from the spinneret. The patterns also show the existence of preferred orientation of the crystalline material, without major change along the spinline.

Take-up speed

The WAXS patterns obtained at a distance of 60 cm from the spinneret, a constant throughput rate of $0.6 \text{ cm}^3\text{min}^{-1}\text{hole}^{-1}$, and different take-up speeds are shown in *Figure 6*, and the corresponding integrated intensity profiles in *Figure 7*. These patterns, and corresponding plots, reveal that crystallinity and crystalline orientation increase with take-up speed.

Throughput rates

The WAXS patterns obtained at a fixed distance from the spinneret and constant take-up speed and different throughput rates, and respective integrated intensity profiles, are shown in *Figure 8*, and *Figure 9*, respectively, and reveal a decrease of crystalline orientation and crystallinity for higher throughput rates, due to a decrease of the stress in the spinline.

Table I. Calculated crystallinity, c-axis orientation and lamellar long period for iPP produced under the conditions indicated.

Throughput rate ($\text{cm}^3\text{min}^{-1}\text{hole}^{-1}$)	Take-up speed (m min^{-1})	Distance from spinneret (cm)	Crystallinity (%)	c-axis orientation	Lamellar long period (nm)
0.6	100	15	a)		d)
		30	42.9	0.268	13.4
		45	59.6	0.263	11.7
		60	65.0	0.247	12.3
0.6	50	60	b) 50.5	0.176	e) --
	100		65.0	0.247	12.3
	200		74.8	0.387	13.1
	400		91.8	0.496	13.7
0.3	100	45	c) 73.8	0.332	f) 12.0
				59.7	0.263
1.2			30.1	0.189	13.6

- a) Parameters derived from data presented in Figures 4 and 5.
- b) Parameters derived from data presented in Figures 6 and 7.
- c) Parameters derived from data presented in Figures 8 and 9.
- d) Parameters derived from data presented in Figures 10 and 11.
- e) Parameters derived from data presented in Figures 12 and 13.
- f) Parameters derived from data presented in Figures 14 and 15.

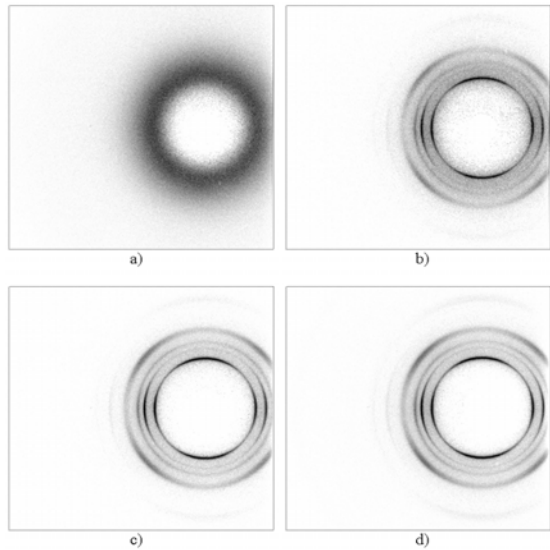


Figure 4. WAXS patterns obtained at distances of a) 15, b) 30, c) 45 and d) 60 cm from the spinneret at a throughput rate of $0.6 \text{ cm}^3 \text{ min}^{-1} \text{ hole}^{-1}$ and take-up speed of 100 m min^{-1} , hole⁻¹ and take-up speeds of: a) 50, b) 100, c) 200, and d) 400 m min^{-1} .

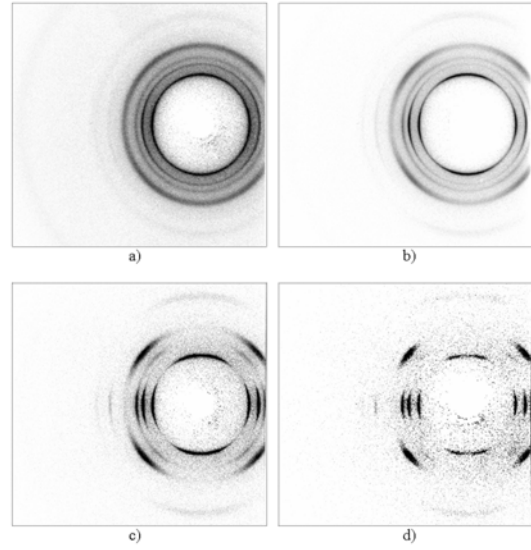


Figure 6. WAXS patterns obtained at a distance of 60 cm from the spinneret at a throughput rate of $0.6 \text{ cm}^3 \text{ min}^{-1} \text{ hole}^{-1}$ and take-up speeds of: a) 50, b) 100, c) 200, and d) 400 m min^{-1} .

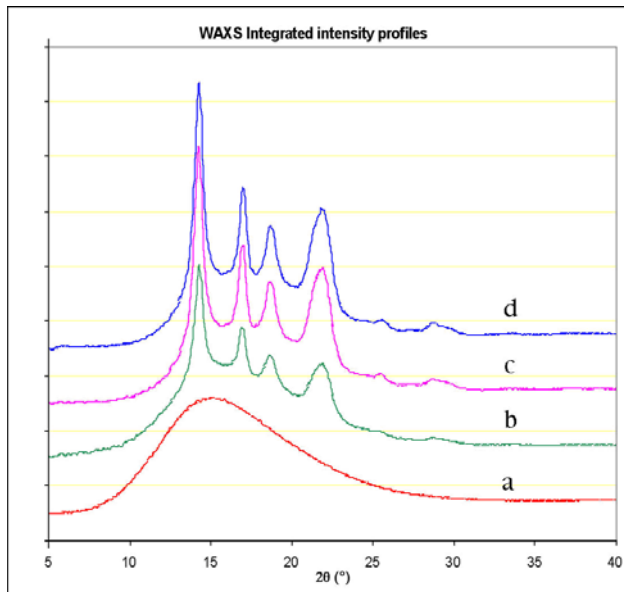


Figure 5. Integrated intensity profiles vs. scattering angle, corresponding to the WAXS patterns obtained at distances of: a) 15, b) 30, c) 45, and d) 60 cm from the spinneret at a throughput rate of $0.6 \text{ cm}^3 \text{ min}^{-1} \text{ hole}^{-1}$ and take-up speed of 100 m min^{-1} . Traces are normalized and shifted vertically for clarity.

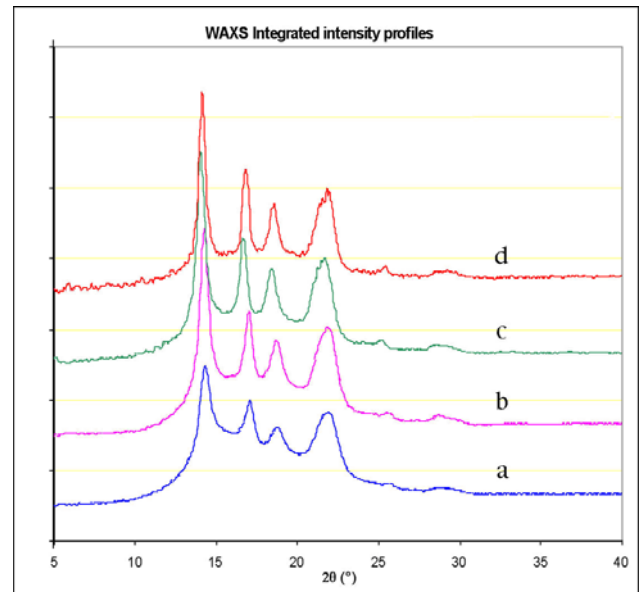


Figure 7. Integrated intensity profiles vs. scattering angle, corresponding to the WAXS patterns obtained at a distance of 60 cm from the spinneret at a throughput rate of $0.6 \text{ cm}^3 \text{ min}^{-1} \text{ hole}^{-1}$ and take-up speeds of: a) 50, b) 100, c) 200, and d) 400 m min^{-1} . Traces are normalized and shifted vertically for clarity.

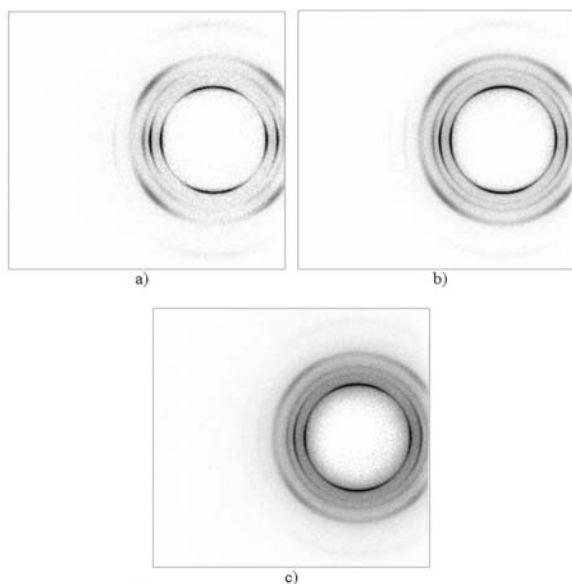


Figure 8. WAXS patterns obtained at a distance of 45 cm from the spinneret at a take-up speed of 100 m min^{-1} , and throughput rates of a) 0.3 , b) 0.6 , and c) $1.2 \text{ cm}^3 \text{ min}^{-1} \text{ hole}^{-1}$.

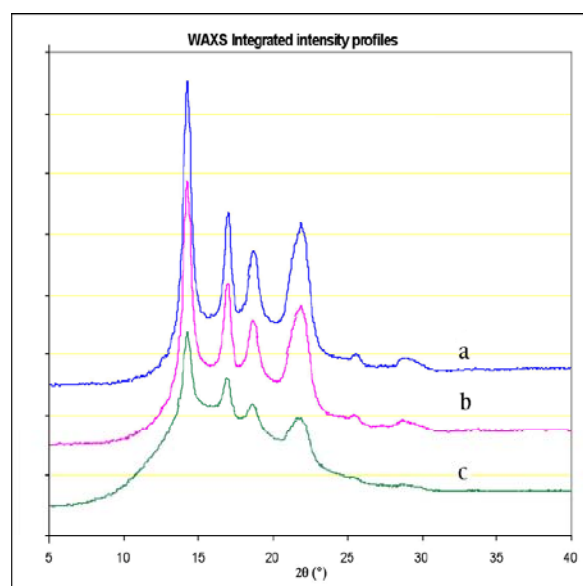


Figure 9. Integrated intensity profiles vs. scattering angle, corresponding to the WAXS patterns obtained at a distance of 45 cm from the spinneret at a take-up speed of 100 m min^{-1} and throughput rates of: a) 0.3 , b) 0.6 , and c) $1.2 \text{ cm}^3 \text{ min}^{-1} \text{ hole}^{-1}$. Traces are normalized and shifted vertically for clarity.

SAXS Patterns

Small angle X-ray patterns were analyzed to monitor changes in the lamellar structure of the polymer fibers as a function of: distance from the exit of the spinneret, take-up speed, and throughput rates. The

lamellar long period distances for these patterns are presented in *Table I*.

Distance from the exit of the spinneret

Small angle X-ray patterns obtained at different distances from the spinneret for all experimental conditions show qualitative changes in the lamellar structure of the polymer fibers. In *Figure 10* a set of SAXS patterns obtained at different distances from the spinneret at a throughput rate of $0.6 \text{ cm}^3 \text{ min}^{-1} \text{ hole}^{-1}$ and take-up speed of 100 m min^{-1} , shows no signal at 15 cm. From 30 cm onwards the patterns reveal a two lobed signal along the meridional direction, characteristic of lamellar structure oriented perpendicular to the fiber axis, with a stable shape, and increasing in intensity. The position of the intensity maximum in the integrated intensity profiles, *Figure 11*, shifts towards higher s values corresponding to a decrease of the lamellar long period with increasing distance from the exit of the spinneret.

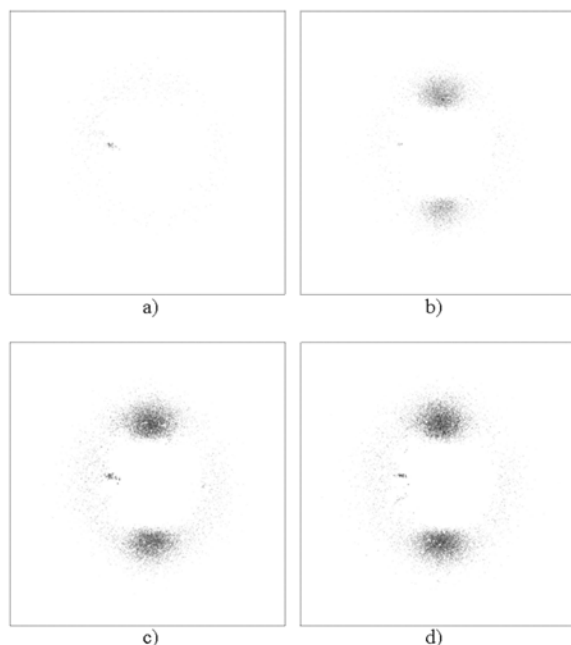


Figure 10. SAXS patterns obtained at distances of: a) 15, b) 30, c) 45 and d) 60 cm from the spinneret at a throughput rate of $0.6 \text{ cm}^3 \text{ min}^{-1} \text{ hole}^{-1}$ and take-up speed of 100 m min^{-1} .

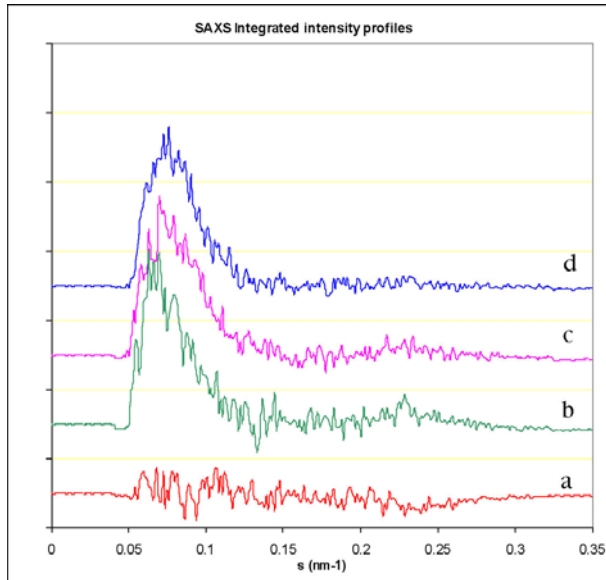


Figure 11. Integrated intensity profiles vs. scattering vector, corresponding to the SAXS patterns obtained at distances of: a) 15, b) 30, c) 45, and d) 60 cm from the spinneret at a throughput rate of $0.6 \text{ cm}^3\text{min}^{-1}\text{hole}^{-1}$ and take-up speed of 100 m min^{-1} . Traces are normalized and vertically shifted for clarity.

Take-up speed

The SAXS patterns obtained at a fixed distance from the spinneret and constant throughput rate with increasing take-up speed, shown in Figure 12, reveal the shape evolution towards a lower spread of intensity in the lateral direction, which can be related to a lower misorientation of the lamellar structure. The position of the intensity maximum in the integrated intensity profiles, Figure 13, shifts towards high s values with decreasing take up speed, corresponding to a decrease of the lamellar long period.

Throughput rates

The SAXS patterns obtained at a fixed distance from the spinneret and constant take-up speed with increasing throughput rate (Figure 14) reveal an increase of the misorientation of the lamellar structure, from 0.3 to $0.6 \text{ cm}^3\text{min}^{-1}\text{hole}^{-1}$. At the flow rate of $1.2 \text{ cm}^3\text{min}^{-1}\text{hole}^{-1}$, the pattern suggests a decrease in the lamellar misorientation which may arise from the low crystallinity of this sample, 30 %, while the crystallinity at the 0.3 and $0.6 \text{ cm}^3\text{min}^{-1}\text{hole}^{-1}$, flow rates were 74 and 60 %, respectively. From the integrated intensity profiles, Figure 15, the lamellar long period increases with increasing throughput rate.

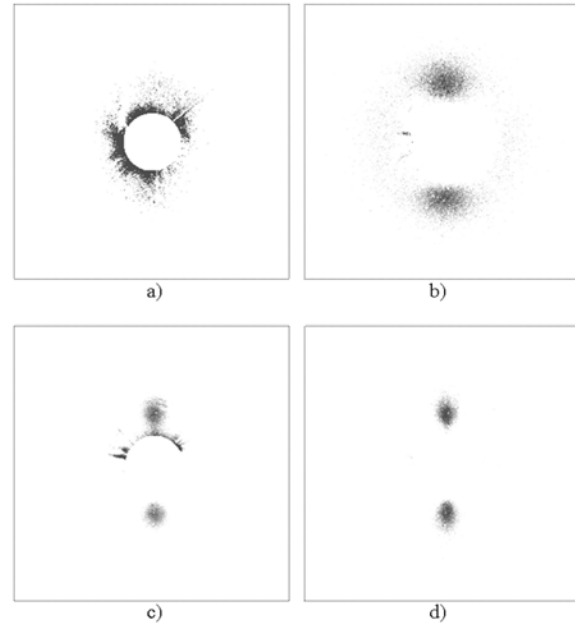


Figure 12. SAXS patterns obtained at a distance of 60 cm from the spinneret at a throughput rate of $0.6 \text{ cm}^3\text{min}^{-1}\text{hole}^{-1}$ and take-up speeds of: a) 50, b) 100, c) 200, and d) 400 m min^{-1} .

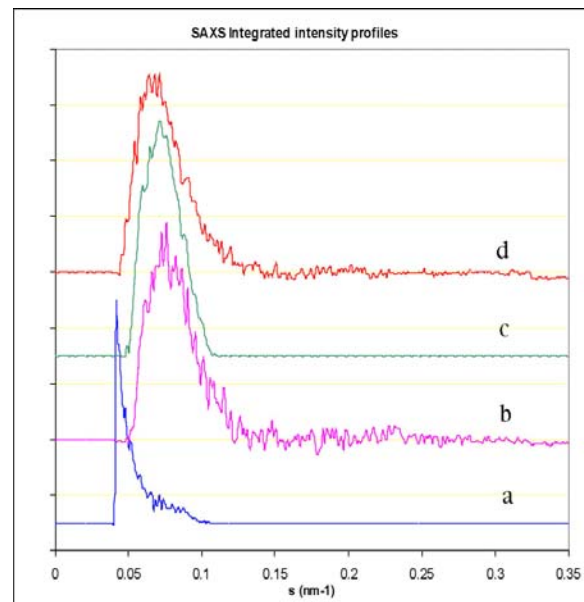


Figure 13. Integrated intensity profiles vs. scattering vector, corresponding to the SAXS patterns obtained at a distance of 60 cm from the spinneret at a throughput rate of $0.6 \text{ cm}^3\text{min}^{-1}\text{hole}^{-1}$ and take-up speeds of: a) 50, b) 100, c) 200, and d) 400 m min^{-1} . Traces are normalized and vertically shifted for clarity.

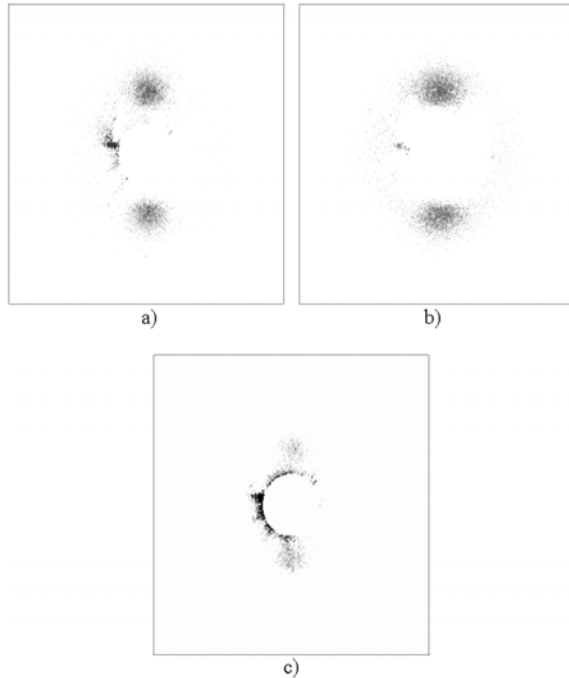


Figure 14. SAXS patterns obtained at a distance of 45 cm from the spinneret at a take-up speed of 100 m min^{-1} and throughput rates of a) 0.3 , b) 0.6 , and c) $1.2 \text{ cm}^3\text{min}^{-1}\text{hole}^{-1}$.

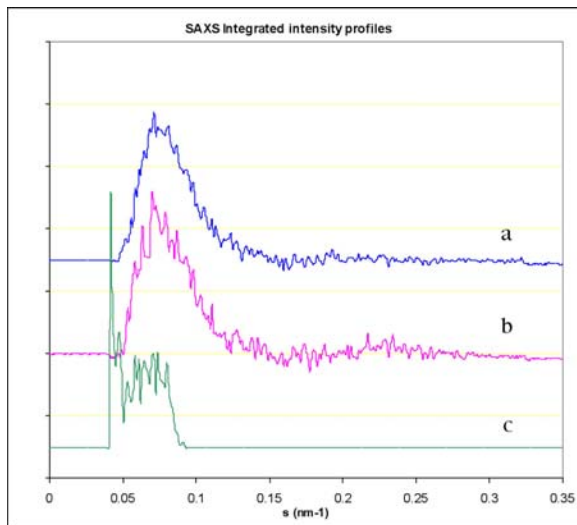


Figure 15. Integrated intensity profiles vs. scattering angle, corresponding to the SAXS patterns obtained at a distance of 45 cm from the spinneret at a take-up speed of 100 m min^{-1} and throughput rates of a) 0.3 , b) 0.6 , and c) $1.2 \text{ cm}^3\text{min}^{-1}\text{hole}^{-1}$. Traces are normalized and vertically shifted for clarity.

CONCLUSIONS

For the first time in situ simultaneous WAXS and SAXS were successfully obtained using a standard

laboratory X-ray source during polymer melt spinning. The in situ X-ray system described has the X-ray source and detectors installed on a vertically mobile platform, allowing measurements to be performed along the spin line.

Crystallinity was found to develop under stress enhanced conditions, evident from the fact that at a given distance from the spinneret at constant throughput rate the crystallinity increased with take-up speed.

Oriented crystallites arise from the melt that presents isotropic X-ray intensity patterns, and the orientation function is almost constant along the spin line, suggesting that crystallite orientation is defined prior to the crystallization process by the chain orientation due to the stress state of the melt during elongational deformation.

SAXS revealed the presence of lamellar structure formed by folded chain crystals and presenting the lamella planes perpendicular to the fiber axis.

WAXS and SAXS signals were detected at the same distance from the spinneret, but in this system any structural feature with long period larger than 20 nm , if present, is obscured by the beam stop.

Automation of data acquisition is an important feature of the system. The requirement for simultaneous detection of WAXS and SAXS mandated the choice of image plates as detectors that are handled successfully by a robotic arm and auxiliary automation.

For in situ experiments exposure times as low as 20 minutes were achieved with a trade off of a less clean top half of the SAXS pattern. Use of a collimation configuration with smaller pin holes should produce cleaner SAXS patterns with equivalent signal intensity using 40 to 60 minutes exposure times.

ACKNOWLEDGMENT

The authors thank Dr. Kathryn A. Stevens of CAEFF - Center for Advanced Engineering Fibers and Films for helpful discussions. This work was supported by the ERC program of the National Science Foundation under Award Number EEC-9731680.

REFERENCES

- [1] Spruiell, J. E. and Bond, E.; Melt spinning of polypropylene. In Karger-Kocsis, J., ed. Polypropylene: An A-Z Reference. Dordrecht: Kluwer Publishers; 1999.

- [2] Hukins D. W. L.; X-ray diffraction by disordered and ordered systems. Oxford: Pergamon Press; 1981.
- [3] Alexander, L. E.; X-ray Diffraction Methods in Polymer Science. New York: Wiley-Interscience; 1969.
- [4] Roe R.-J.; Methods of X-ray and neutron scattering in polymer science. New York: Oxford University Press; 2000.
- [5] Guinier, A.; X-ray diffraction in crystals, imperfect crystals, and amorphous bodies. San Francisco, CA: W.H.Freeman; 1963.
- [6] Sheehan, W. C. and Cole, T. B.; Production of super-tenacity polypropylene filaments. J Appl Polym Sci; 8; 2359-2388; 1964.
- [7] Dees, J. R. and Spruiell, J. E.; Structure Development During Melt Spinning of Linear Polyethylene Fibers. J Appl Polym Sci; 18; 1053-1078; 1974.
- [8] Samuels, R. J.; Structured Polymer Properties: The Identification, Interpretation, and Application of Crystalline Polymer Structure. New York: John Wiley & Sons, Inc.; 1974.
- [9] Spruiell, J. E. and White, J. L.; Structure development during polymer processing: Studies of the melt spinning of polyethylene and polypropylene fibers. Polym Eng Sci; 15; 660-667; 1975.
- [10] Bankar, V., Spruiell, J.E., White, J.L.; Melt spinning of isotactic polypropylene: Structure development and relationship to mechanical properties. J Appl Polym Sci; 21; 3003-3022; 1977.
- [11] Bankar, V., Spruiell, J. E. and White, J. L.; Melt-spinning dynamics and rheological properties of nylon 6. J Appl Polym Sci; 21; 2135-2155; 1977.
- [12] Bankar, V., Spruiell, J. E. and White, J. L.; Melt Spinning of Nylon 6: Structure Development and Mechanical Properties of As-Spun Filaments. J Appl Polym Sci; 21; 2341-2358 1977.
- [13] Danford, M. D., Spruiell, J. E. and White, J. L.; Structure Development in the Melt Spinning of Nylon 66 Fibers and Comparison to Nylon 6. J Appl Polym Sci; 22; 3351-3361; 1978.
- [14] White, J. L. and Cakmak, M.; Orientation development and crystallization in melt spinning of fibers. Adv Polym Tech; 6; 295-337; 1986.
- [15] Lu, F.-M. and Spruiell, J. E.; The influence of resin characteristics on the high speed melt spinning of isotactic polypropylene. II. On-line studies of diameter, birefringence, and temperature profiles. J Appl Polym Sci; 34; 1541-1556; 1987.
- [16] Katayama, K., Amano, T. and Nakamura, K.; Structural Formation during melt spinning process. Kolloid Z. Z. Polym; 226; 125-134; 1968.
- [17] Haberkorn, H., Hahn, K., Breuer, H., Dorrer, H.-D., Matthies, P.; On the neck-like deformation in high-speed spun polyamides. J Appl Polym Sci; 47; 1551-1579; 1993.
- [18] Hsiao, B. S., Barton, R. and Quintana, J.; Simple on-line X-ray setup to monitor structural changes during fiber processing. J Appl Polym Sci; 62; 2061-2068; 1996.
- [19] Cakmak, M., Teitge, A, Zachmann, H.G., White, J.L.; On-line small-angle and wide-angle X-ray scattering studies on melt-spinning poly(vinylidene fluoride) tape using synchrotron radiation. J Polym Sci Pol Phys; 31;371-381; 1993.
- [20] Terrill, N.J., Fairclough, J.P.A., Towns-Andrews, E., Komanschek, B.U., Young, R.J., Ryan, A.J.; Density fluctuations: the nucleation event in isotactic polypropylene crystallization. Polymer; 39;2381-2385; 1998.
- [21] Samon, J.M., Schultz, J.M., Wu, J., Hsiao, B.S., Yeh, F., Kolb, R.; Study of the Structure Development during the Melt Spinning of Nylon 6 Fiber by On-Line Wide-Angle Synchrotron X-ray Scattering Techniques. J Polym Sci Pol Phys; 37;1277-1287; 1999.
- [22] Samon, J.M., Schultz, J.M., Wu, J., Hsiao, B.S., Seifert, S., Stribeck, N., Gurke, I., Collins, G., Saw, C.; Structure development during the melt spinning of polyethylene and poly(vinylidene fluoride) fibers by in situ synchrotron small- and wide-angle X-ray scattering techniques. Macromolecules; 32; 8121-8132; 1999.
- [23] Samon, J.M., Schultz, J.M., Hsiao, B.S., Wu, J., Khot, S.; Structure development during melt spinning and subsequent annealing of polybutene-1 fibers. J Polym Sci Pol Phys; 38; 1872-1882; 2000.
- [24] Kolb, R., Seifert, S., Stribeck, N., Zachmann, H.G.; Simultaneous measurements of small- and wide-angle X-ray scattering during low speed spinning of poly(propylene) using synchrotron radiation. Polymer; 41; 1497-1505; 2000.
- [25] Kolb, R., Seifert, S., Stribeck, N., Zachmann, H.G.; Investigation of the high speed spinning process of poly(ethylene terephthalate) by means of synchrotron X-ray diffraction. Polymer; 41; 2931-2935; 2000.
- [26] Schultz, J. M., Hsiao, B. S. and Samon, J. M.; Structural development during the early stages of polymer melt spinning by in-situ synchrotron X-ray techniques. Polymer; 41; 8887-8895; 2000.

- [27] Samon, J.M., Schultz, J.M., Hsiao, B.S., Khot, S., Johnson, H.R.; Structure development during the melt spinning of poly(oxymethylene) fiber. *Polymer*; 42; 1547-1559; 2001.
- [28] Edie, D.D., Ellison, M.E., Pennington, W.T. and Zumbrennen, D.A.; NSF Proposal for Portable On-line X-ray Diffraction System. 1999.
- [29] Spectre – X ray system control software; version 1.3.04, Rigaku/Molecular Structure Corporation, The Woodlands, TX; 2001.
- [30] Polar – X-ray data analysis software manual. Stonybrook Technology and Applied Research, Inc, NY, USA, v 1.04; 2003
- [31] Wilchinsky, Z.W.; Measurement of Orientation in Polypropylene Film. *J Appl Phys*; 31; 1969-1972; 1960.
- [32] Koike, Y. and Cakmak, M.; Real time development of structure in partially molten state stretching of PP as detected by spectral birefringence technique. *Polymer*; 44; 4249-4260; 2003.

AUTHORS' ADDRESSES

Michael S. Ellison, Ph.D.

Clemson University
School of Materials Science and Engineering
161 Sirrine Hall, Box 340971
Clemson, SC 29634-0971
USA

Paulo E. Lopes, Ph.D.

Clemson University
Center for Advanced Engineering Fibers and Films
(CAEFF) and Department of Chemistry
Clemson, SC 29634
USA

William T. Pennington, Ph.D.

Clemson University
Department of Chemistry and Center for Advanced
Engineering Fibers and Films (CAEFF)
Clemson, SC 29634
USA